High-speed odor transduction and pulse tracking by insect olfactory receptor neurons

Paul Szyszka[a,b,1], Richard C. Gerkin[a], C. Giovanni Galizia[b], and Brian H. Smith[a]

[a]School of Life Sciences, Arizona State University, Tempe, AZ 85287; and [b]Department of Biology, University of Konstanz, 78464 Konstanz, Germany

Edited by Lynn M. Riddiford, Howard Hughes Medical Institute, Janelia Farm Research Campus, Ashburn, VA, and approved October 17, 2014 (received for review June 27, 2014)

Sensory systems encode both the static quality of a stimulus (e.g., color or shape) and its kinetics (e.g., speed and direction). The limits with which stimulus kinetics can be resolved are well understood in vision, audition, and somatosensation. However, the maximum temporal resolution of olfactory systems has not been accurately determined. Here, we probe the limits of temporal resolution in insect olfaction by delivering high frequency odor pulses and measuring sensory responses in the antennae. We show that transduction times and pulse tracking capabilities of olfactory receptor neurons are faster than previously reported. Once an odorant arrives at the boundary layer of the antenna, odor transduction can occur within less than 2 ms and fluctuating odor stimuli can be resolved at frequencies more than 100 Hz. Thus, insect olfactory receptor neurons can track stimuli of very short duration, as occur when their antennae encounter narrow filaments in an odor plume. These results provide a new upper bound to the kinetics of odor tracking in insect olfactory receptor neurons and to the latency of initial transduction events in olfaction.

olfaction | olfactory receptor neurons | odor transduction | temporal resolution | insect

Odors carried in air plumes quickly break up into thin filaments that spread out across short distances from an odor source (1). The ability to track the temporal structure of filaments in an odor plume is essential for insects to segregate concurrent odors that arise from different sources (2–6). However, it is not clear whether signal transduction times and tracking rates of olfactory receptor neurons (ORNs) are fast enough to allow animals to use the higher frequency components of information present in odor plumes. Insect odor-guided behavior is remarkably robust against the spatial and temporal variability inherent in olfactory stimuli. For example, moths and beetles use temporal stimulus cues to segregate concurrent odors from closely spaced sources (2–5), and honey bees can detect 6-ms asynchrony in the onset of concurrent odor stimuli and use this onset asynchrony to segregate concurrent odors (6, 7). These observations of fast temporal resolution challenge the frequent notion that olfaction has slow integration times relative to other senses. Olfactory transduction speed has never been measured directly, and estimates range from 10 to 30 ms (8–11). Previous studies suggest that the maximum pulse tracking frequency of ORNs is species specific and ranges from 5 to 50 Hz (12–19). However, these numbers do not match the high temporal resolution observed in behavioral studies (2–7).

We tested the limits of olfactory transduction speed and pulse tracking in five different insect species by measuring ORN population responses using electroantennogram (EAG) recordings. The amplitude and dynamics of EAG signals are proportional to the number of sensilla stimulated (20). They are also affected by receptor current amplitude, positions of the neurons relative to the recording electrode, and electrical properties of the antenna itself (21). With appropriate odorless controls for electrical and mechanical artifacts, measuring EAG signals provides reliable estimates of transduction latencies and pulse tracking ability of ORNs.

Results

We constructed an odor delivery device capable of delivering high frequency pulses (Fig. 1*A* and Fig. S1). Using titanium tetrachloride ($TiCl_4$) in separate experiments to visualize stimuli, we estimated that this device delivers odor pulses to the antenna in 3.3 ± 0.3 ms (mean ± SD) after triggering the valve to open (Fig. 1*C*). We produced repetitive pulses at frequencies of up to 200 Hz. To control for responses to mechanical stimuli in experiments with olfactory stimuli, we alternated odor and blank (odorless) stimuli and subtracted a blank control from the preceding odor-evoked EAG signal (Fig. S2).

Odor-evoked mean EAG responses began between 1.6 and 26.4 ms after odors arrived at the antenna (Fig. 1*B*). EAG response latency depended on odor identity and decreased with increases in concentration (Fig. 1*C*). The shortest EAG response onset latencies ranged from 1.6 ms in locusts to 4.6 ms in moths, and there were no systematic differences between general odors and species-specific sex or alarm pheromones (Fig. 1*C*).

To test antennal pulse tracking capability we applied a 1-s-long series of odor pulses at intervals ranging from 6 to 100 ms (167–10 Hz; Figs. 2 and 3). Pulse tracking capability decreased with increasing pulse frequency and differed between odorants and concentrations, and the maximum pulse tracking frequencies ranged from 50 Hz in the orange spotted cockroach to 125 Hz in the honey bee and locust (Fig. 3 *A* and *B*; see Fig. S3*A* for variability across antennae).

Filaments in natural odor plumes arrive at random intervals and persist for random durations (1). We mimicked this type of pattern by applying a 10-s-long broadband frequency stimulus train with random pulse durations and intervals (Fig. 4*A*). Insect EAG responses have approximately linear frequency response functions over a wide frequency range, and coherence analysis

Significance

How fast can animals smell? Whereas we know how fast our eyes are (in the cinema, images at 24 Hz fuse for humans, whereas our retina can resolve flickers at more than 100 Hz), olfactory perception is believed to be slow. After all, we take a sniff and later another one. Odor plumes in the air, however, can fluctuate at a millisecond time scale. Here, we show that insect olfactory receptor neurons can have response latencies shorter than 2 ms and resolve odorant fluctuations at more than 100 Hz. This high temporal resolution could facilitate odor-background segregation, and it has important implications for underlying cellular processes (transduction), ecology (odor recognition), and technology (development of fast sensors).

Author contributions: P.S., R.C.G., and B.H.S. designed research; P.S. performed research; P.S., R.C.G., C.G.G., and B.H.S. analyzed data; and P.S., R.C.G., C.G.G., and B.H.S. wrote the paper.

The authors declare no conflict of interest.

This article is a PNAS Direct Submission.

[1]To whom correspondence should be addressed. Email: paul.szyszka@uni-konstanz.de.

This article contains supporting information online at www.pnas.org/lookup/suppl/doi:10.1073/pnas.1412051111/-/DCSupplemental.

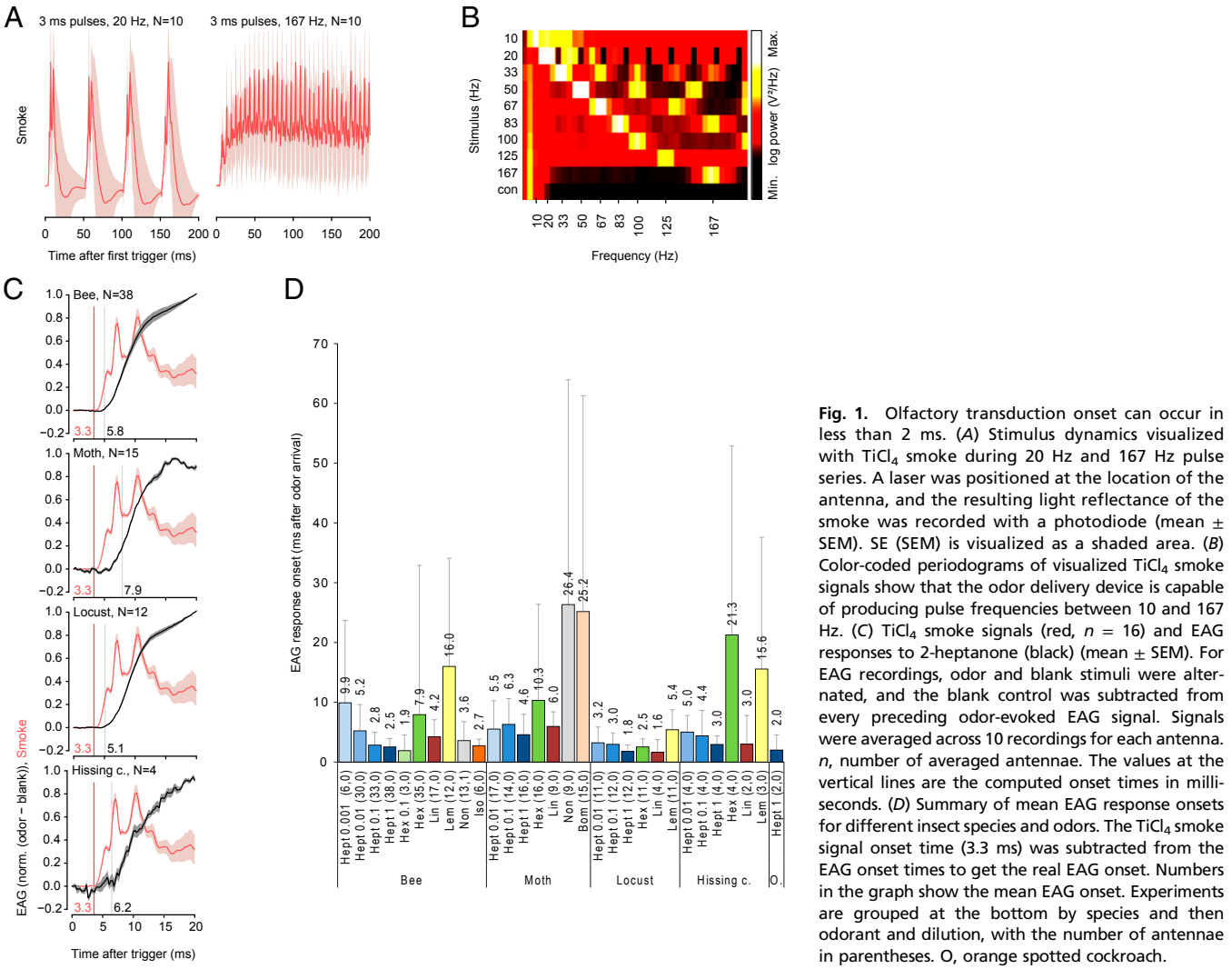

Fig. 1. Olfactory transduction onset can occur in less than 2 ms. (*A*) Stimulus dynamics visualized with $TiCl_4$ smoke during 20 Hz and 167 Hz pulse series. A laser was positioned at the location of the antenna, and the resulting light reflectance of the smoke was recorded with a photodiode (mean ± SEM). SE (SEM) is visualized as a shaded area. (*B*) Color-coded periodograms of visualized $TiCl_4$ smoke signals show that the odor delivery device is capable of producing pulse frequencies between 10 and 167 Hz. (*C*) $TiCl_4$ smoke signals (red, n = 16) and EAG responses to 2-heptanone (black) (mean ± SEM). For EAG recordings, odor and blank stimuli were alternated, and the blank control was subtracted from every preceding odor-evoked EAG signal. Signals were averaged across 10 recordings for each antenna. n, number of averaged antennae. The values at the vertical lines are the computed onset times in milliseconds. (*D*) Summary of mean EAG response onsets for different insect species and odors. The $TiCl_4$ smoke signal onset time (3.3 ms) was subtracted from the EAG onset times to get the real EAG onset. Numbers in the graph show the mean EAG onset. Experiments are grouped at the bottom by species and then odorant and dilution, with the number of antennae in parentheses. O, orange spotted cockroach.

provides a tool to measure the ORNs' temporal resolution (15, 16). We identified the antennae's temporal resolution as the maximum stimulus frequencies at which the coherence between the EAG response and the $TiCl_4$ smoke signal was significant at the 5 sigma level (Fig. 4*B*). The temporal resolution differed between odorants and increased with concentration (Fig. 4*C*; see Fig. S3*B* for variability across antennae). Across insects, the maximum temporal resolution ranged from 114 to 473 Hz (8.8- to 2.1-ms interpulse intervals).

Odor sampling is ongoing during behavior, but ORNs adapt over a variety of timescales (22, 23). We therefore asked whether the fast EAG kinetics we observed adapt across odor pulses and how this adaptation would affect the maximum temporal resolution. For honey bee EAGs, the temporal resolution was higher during the late odor response than during the initial odor response, whereas for the other insect species the temporal resolution appeared to be invariant to stimulus duration (Fig. 4*D* and Fig. S4).

To further demonstrate that insect antennae are capable of resolving fast changes in odor concentration, we configured the odor delivery valve to play the notes of a children's song about bees (Fig. S5 and Audio File S1), releasing a barrage of odor pulses (2-heptanone) at frequencies between 100 and 200 Hz (1/interval between pulse onsets) with each note (Audio File S2). We recorded the EAG during this song, and subtracted the corresponding EAG when the same song was played by using blank control pulses. In this blank-subtracted EAG, the original song was clearly recognizable (Audio File S3). Thus, insect antennae can follow olfactory stimuli in a frequency range high enough to significantly overlap that of the human auditory system.

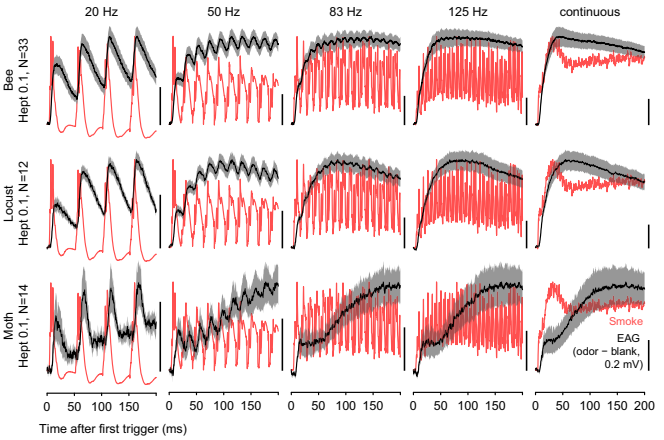

Fig. 2. EAG responses in different insect species. EAG responses (black, mean ± SEM) to 20, 50, 83, and 125 Hz pulse series and a continuous stimulus in three insect species are shown. $TiCl_4$ smoke signals (red) show the stimulus dynamic.

Discussion

Our data show that the initial olfactory transduction process requires less than 2 ms. This short transduction time contradicts previous studies that suggested olfactory transduction times between 10 and 30 ms (8–11). What makes olfactory transduction fast? Olfactory transduction involves several steps, including diffusion of the odorant molecule through the antenna surface, its binding to an odorant-binding protein (OBP), diffusion through the aqueous sensillar lymph to an ORN dendrite, activation of an odor receptor, and opening of ion channels (11, 24, 25). Modeling studies suggest that diffusion can delay the initial ORN response by 10 ms (11, 26). Using available data about OBPs and the sensillum lymph, we estimate that >17% of the odorant molecules should reach the ORN dendrite by 3D diffusion alone within 1 ms of encountering the lymph surface (*SI Materials and Methods*). Diffusion speed might be further increased by pore tubules that connect the sensillum pore with the ORN dendrite (8, 27, 28). Moreover, OBPs occur at high concentrations (10 mM) in the sensillum lymph of insects (29, 30), which improves ORN sensitivity (25) and might decrease transduction time.

Insect olfactory transduction mechanisms include both ionotropic and metabotropic components (10, 24, 31, 32). Although ionotropic transduction is believed to be faster, both transduction mechanisms are capable of high temporal resolution. For example, insect photoreceptor cells are metabotropic and reach temporal resolutions of 300 Hz (33). Unlike resolution, however, the transduction latencies of most metabotropic receptors are at least one order of magnitude longer than the few millisecond short transduction latencies that we found. Metabotropic olfactory receptors of vertebrates, for example, have minimum transduction latencies between 50 and 150 ms (34, 35), and the fastest metabotropic receptors in photoreceptors of the fly have a minimum transduction latency of 20 ms (36). Therefore, the fast transduction latencies we found here—4.6 ms or less across all tested species—support the hypothesis that the primary transduction mechanism for insect odor receptors is ionotropic.

Single ORNs typically have spike rates well below 350 Hz (8, 9, 22, 23). We found that EAG responses can follow odor fluctuations that exceed 350 Hz. It is therefore likely that higher pulse frequencies are encoded by the volley principle (37): Single ORNs might respond to repetitive odor pulses intermittently so that the combined ensemble activity is able to track frequencies that exceed the tracking capabilities of a single ORN.

Previous studies reported maximum odor-tracking frequencies between 5 and 50 Hz in EAG and single ORN recordings (12–14, 16, 18, 38, 39) and between 10 and 30 Hz in olfactory interneurons in the antennal lobe (17, 40, 41). These lower maximum pulse tracking frequencies might reflect the low-pass filter properties of the odor delivery devices. Odor delivery devices typically act as a low-pass filter because of the dead volume in the odor chamber of the device, and because odorants adhere to surfaces used to construct the device (23). In some studies, odor stimuli were given as randomized fluctuating pulses and monitored at frequencies up to ~100 Hz, still limiting the investigation of pulse tracking to values below its biological limits (15, 16).

Fast olfactory transduction speeds could facilitate the recognition of a target odor in the presence of background odors. Insects rely on olfaction to localize resources such as food, mates, or hosts (42). Finding an odor source poses a particular challenge: Odor plumes break into thin filaments, and relevant target odors intermingle with background odors (43). Insects and slugs can exploit temporal differences in the arrival of odorants to segregate a target odor from background odors that emanate from different sources (2, 3, 5–7, 44–46). In this task, fast olfactory transduction might enable animals to resolve short differences in the arrival of a target odor and background odors.

We cannot directly extrapolate our results to mammalian olfaction, because both olfactory transduction mechanisms and temporal constraints differ across phyla. For example, mammals impose a sniffing rhythm onto odor samples that they take from the environment (47). Nevertheless, high temporal resolution might be used by mammals to detect minor temporal differences in adsorption of odorants along the mucosal lining, which could allow odor identification based on odorant-specific ORN response latencies (48).

Finally, the fast temporal resolution of insect olfaction we report here has implications for the development of artificial odor sensors for odor-source localization. The segregation of a target odor from background odors via temporal stimulus cues (2–4, 6, 7, 49) requires fast sensor operation. Current artificial odor sensors, e.g., metal oxide sensors, have a temporal resolution lower than that of the antennae investigated here (50). Thus, hybrids of engineered devices with biological sensors might improve the performance of new devices (51–53).

Materials and Methods

Animals. Experiments were performed on adult orange spotted cockroach *Blaptica dubia* of both sexes, hissing cockroaches *Gromphadorhina portentosa* of both sexes, male locusts *Schistocerca americana*, female forager honey bees *Apis mellifera*, and male moth *Manduca sexta* 3–8 d after hatching. Moth EAGs were recorded during the night.

Odorants. Odorants were used pure or diluted in mineral oil (Sigma-Aldrich). Odorant dilutions were prepared fresh every 4 wk. All dilutions are reported as parts per one part of mineral oil. The odorants used were as follows: the honey bee alarm pheromones and plant odors 2-heptanone (dilutions: 0.001, 0.01, 0.1, undiluted) and isopentylacetat (0.032); a 1:1 mixture of the synthetic *M. sexta* sex pheromone components E,Z-10,12-hexadecadienal and E,Z-11,13-pentadecadienal (Bom, 10 ng/μL); and the plant odors linalool (undiluted) 1-hexanol (0.1, undiluted); 1-nonanol (undiluted); and lemon oil (0.1). Pure mineral oil served as blank control. One microliter of Bom and 10 μL of all other odorant solutions were loaded onto a cellulose strip (Sugi, REF 31003; Kettenbach) located in a 3-mL syringe (Norm-Ject; Henke-Sass, Wolf), adjusted to 2.5-mL syringes were prepared daily.

Odorant Delivery Device. We built an odor delivery device with minute dead space and adsorbent surfaces to ensure that the odor dynamics at the antenna reflected the dynamics of the valve as faithfully as possible (Fig. S1*A*). Odor stimuli were delivered with a three-way solenoid valve (LFAA1200118H; Lee) (Fig. S1*A*). Odor syringes were supplied with air via a manifold that was designed to minimize cross-contamination. The manifold was a Teflon septum equipped glass vial (20 mL of headspace vial; Schmidlin Labor and Service), which was connected to the odor syringe and the valve via injection needles (1.20 × 40 mm, Sterican; Braun). The needles served as nonreturn valves. This odor delivery device was supplied with pressurized, charcoal filtered, dry air. The air stream was adjusted to 260 mL/min by a flow meter. The three-way solenoid valve controlled the odor pulses by diverting air from the manifold to the odorant syringe. The valve was switched with a spike-and-hold driver circuit to minimize opening time. The valve was shielded with an iron cage. A stainless steel tube (inner diameter 1.2 mm) served as outlet. The air speed at the outlet of the steel tube was 383.15 cm/s.

The distance between antenna and the gate of the valve was 15.6 mm. The gate of the valve started moving 0.4 ms after the electrical trigger signal that switches the valve (Fig. S1*B*). Assuming a laminar airflow and no pressure changes, the odor would arrive 4.47 ms after the trigger signal that operated the valve (0.4-ms valve delay plus 4.07-ms air travel time). For measuring the movement of the valve gate, a valve was cut open and a laser beam was directed in a 45° angle onto the gate and a photodiode with a 0.2-mm pinhole was placed in the focus of the reflected laser beam. Movement of the valve caused changes in the light intensity and was visible as changes in the photodiode signal. The analog photodiode signal was digitized with the same recording setup and settings that were used for the EAG recordings (see below).

The arrival time and dynamics of the odor stimulus were measured with a photodiode, a green laser, and $TiCl_4$ smoke as tracer substance (Fig. S1*C*). The laser was positioned at the location of the antenna, perpendicular to the airflow, and the reflectance of the smoke was recorded with a photodiode. One microliter of $TiCl_4$ solution was placed in an odor syringe. Before

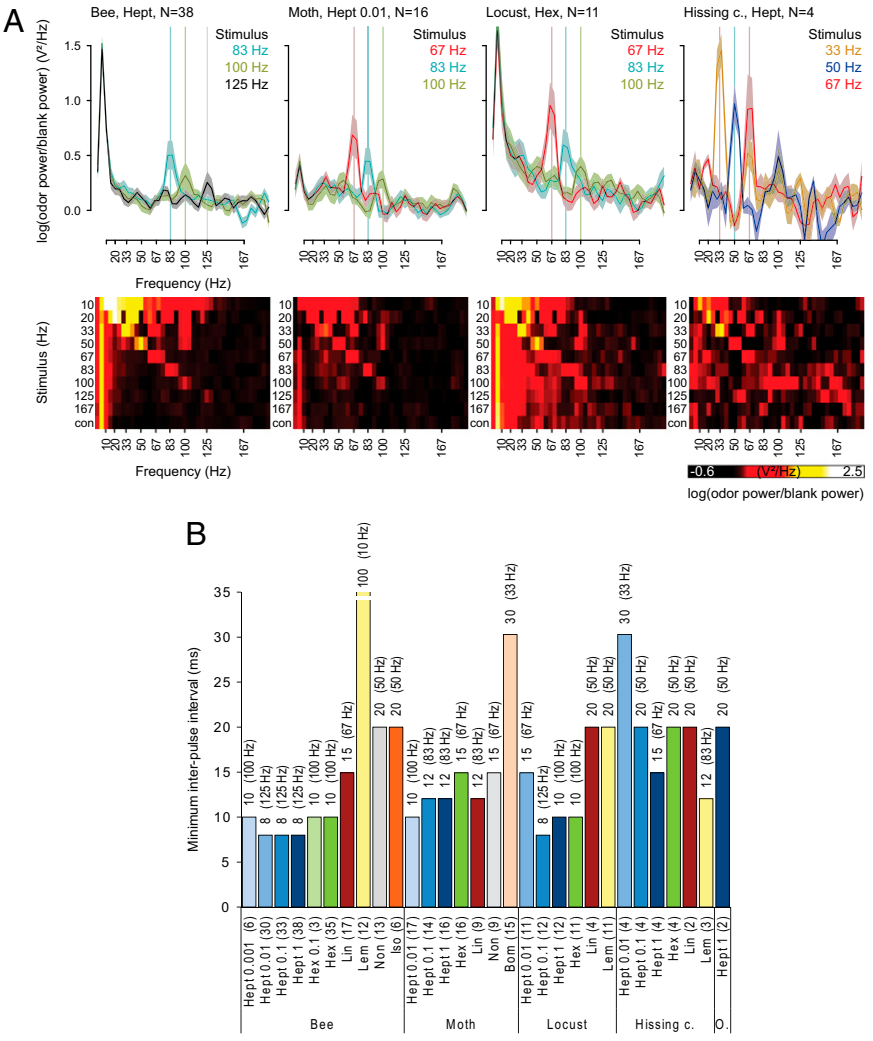

Fig. 3. Antennal responses track pulses at 125 Hz in a 1-s-long odor stimulus. (*A*) Periodograms (mean ± SEM) of the EAG responses for the three highest resolved pulse frequencies for different odors in different insect species, and color-coded periodograms for all pulse series for the same species-odor combination. A peak in the periodogram indicates that the EAG response followed that stimulus frequency. (*B*) Temporal resolution of EAG responses quantified as the minimum interpulse interval in milliseconds (1/maximum pulse frequency) that an EAG response could follow. Minimum interpulse intervals were determined by locating the peak of the average periodogram in a ± 20-Hz window around the stimulus frequency. Pulse following was ascertained if the negative SE of the peak location rose above the positive SE of the trough location within that window. The corresponding pulse tracking frequencies are given in parentheses. The number of antennae is given in parentheses above the odorant.

starting the pulse sequence, the valve was opened for 1 s (from 2,000 to 1,000 ms before pulse onset) to fill the valve with fresh smoke.

To estimate the effect of diffusion on the relative arrival times of odorants and $TiCl_4$ and, thus, on EAG onset, we calculated the time needed for a small fraction (0.1%) of the molecules to reach the antenna by diffusion alone. The SD or root-mean-square displacement of molecules along one dimension in a diffusion profile at time t is given by square root ($2 \times D \times t$). The diffusion coefficient, D, in air for the odorant from our panel with the lowest-latency EAG response, 2-heptanone, is ∼7.3 mm^2/s. By definition, 0.1% of molecules will be found at least ∼2.33 SDs from the diffusion source, a distance we take to be the 15.6 mm from the valve gate to the antenna. Solving gives a SD of 6.7 mm, and a corresponding diffusion time of 6.7 $mm^2/(2 \times 7.3\ mm^2/s) = 0.46$ s. In contrast, the $TiCl_4$ smoke reaches the antenna within 3.3 ms. Therefore, odorant delivery via diffusion is more than 100 times slower than odorant delivery via airflow and, thus, for our odor delivery device, diffusion in air is not a relevant concern for the early EAG response.

Odorant Stimuli. Odorants were delivered as continuous 1-s long pulses, 1-s long trains of 3-ms-long pulses at frequencies of 10, 20, 33, 50, 67, 83, 100, 125, and 167 Hz, or 10-s-long broadband frequency stimulus trains with theoretically flat power spectrum. The power spectrum of the actual broadband stimulus is colored because of the noninstantaneous impulse response of the valve (Fig. S1*D*). The broadband frequency stimulus was generated by constructing a 12-bit M-sequence, scaling to achieve a minimum "on" time of 3 ms, and then selecting a random 10-s segment. It consisted of 12,330 pulses between 3 and 39 ms in length, with interpulse intervals (onset to onset) ranging from 56 to 6 ms.

The notes of the song "Biene" (Fig. S5 and Audio File S1) were encoded as pure tones, such that the first note "C5" was tuned to ∼"D3," or 143 Hz. These were played into the odor delivery device by opening and closing the valve at the corresponding frequencies ranging between 100 and 200 Hz, with a fixed number of pulses representing the lengths of the notes (Audio File S2). The resulting performance of the song by the valve thus matches the sheet music. EAG responses due to pressure from the air pulses were accounted for by recording in both the presence and the absence of an odorant (2-heptanone) loaded into the olfactometer and taking the difference. The resulting subtracted EAG thus reflects a purely odor-driven response. This EAG response was averaged across four antennae (two honey bee and two moth antennae), and band-pass filtered (40–400 Hz) to remove subauditory slow changes in the EAG and to denoise the response. The resulting waveform was upsampled and multiplied by a constant to produce a sound file, but the spectral peaks were unaltered (Audio File S3).

EAG Recordings. Antennae were cut and mounted with conductive gel (lubricating jelly; CVS pharmacy) between the two poles of a custom-made silver electrode. For EAG recordings from honey bees, the scapus was cut at the flagellum joint and removed (Fig. S1*A*). For other insects, 5-mm-long antenna pieces were used. Differences in the dynamic properties of the EAG responses between insect species might reflect differences in the number of stimulated ORNs and difference in the electrical properties of the antenna preparations. Recordings started 15 min after mounting the antennae. The signal was amplified, band-pass filtered to select the 0.1–9 kHz range, and digitized at a sampling rate of 30 KHz with an extracellular recording system (Cheetah16; Neuralynx). Experiments were performed at 28 °C.

Data Analysis. Odor-evoked EAG signals were derived by subtracting EAG signals in trials by using blank control stimulus from corresponding signals in trials with odor stimulus (Fig. S2*A*). Blanks recorded in trials before or after

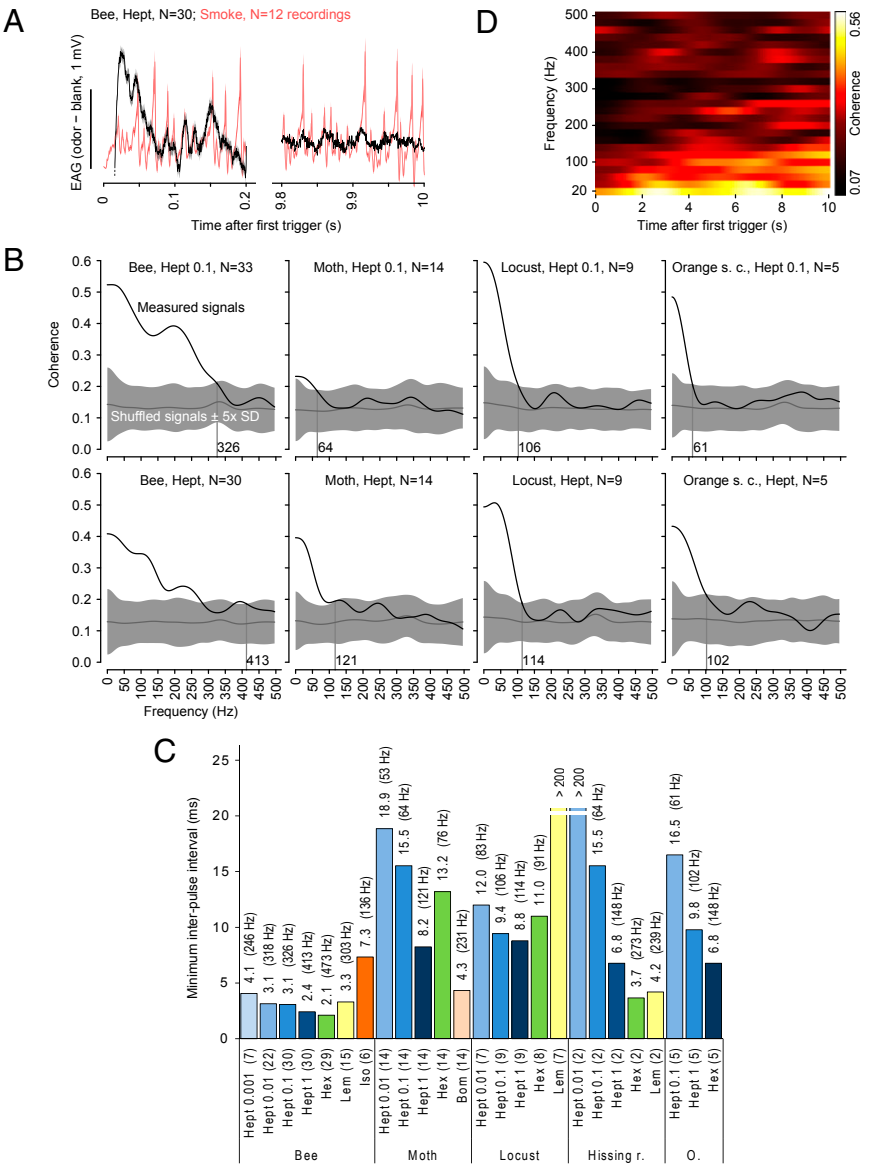

Fig. 4. Antennal responses track odor fluctuations in the hundreds of Hertz range during a persistent broadband stimulus. (*A*) $TiCl_4$ smoke signals (red, n = 12) and odor-evoked EAG responses (black, 20 Hz high-pass filtered, onset truncated, n = 30) (mean ± SEM) during 0–0.2 and 9.8–10 s of a 10-s-long broadband frequency stimulus train with random pulse durations and intervals. (*B*) Coherence between mean EAG responses and $TiCl_4$ smoke signals (black) and coherence between mean EAG response and a shuffled $TiCl_4$ smoke signal (gray, mean ± 5 SD). The first 1,000 and the last 100 ms of the 10-s-long broadband stimulus were skipped to avoid onset/offset effects. Coherence was defined significant when it was larger than the coherence for the shuffled data plus 5 SD. Values at the vertical lines are the maximum frequencies at which the EAG response shows significant coherence. (*C*) Temporal resolution of EAG responses quantified as the minimum interpulse interval in milliseconds (1/maximum pulse frequency) at which the coherence was significant, i.e., larger than the coherence for the shuffled data plus 5 SD. The corresponding pulse tracking frequencies are given in parentheses. Experiments are grouped at the bottom by species and then odorant and dilution, with the number of antennae in parentheses. (*D*) Time-resolved, color-coded coherence between the mean honey bee EAG response to undiluted 2-heptanone and the mean $TiCl_4$ smoke signal (same data as in Fig. 4*A*). The time-resolved coherence indicates the degree to which the EAG response is phase-locked to the fluctuations of the odor concentration, as opposed to merely matching the frequency. Substantial coherence at high frequencies is visible throughout the odor presentation, indicating that tracking can persist for several seconds.

odor trials had similar properties, i.e., no long-term odor adaptation was observed. There was a small nonolfactory EAG signal that occurred before the odor reaches the antenna and that coincided with the closing of the valve (Fig. S2*B*). The amplitudes of this nonolfactory signal ranged between 12 and 36 μV compared with odor-evoked signals between 73 and 568 μV. We assume that these signals are inductive artifacts that arise from current flow in the coil of the valve when the valve closes. The subtraction of the blank evoked from the odor-evoked EAG signal removed the stimulus artifacts in the analyzed data (Fig. S2*B*).

Odor-evoked EAG signals were baseline-subtracted and valve-triggered averages were constructed by taking the mean EAG response centered on the onset of the first pulse of each pulse train.

EAG response or $TiCl_4$ signal onset times (Fig. 1 *C* and *D*) were determined by using the continuous stimulus and the first pulse of each of the 10- to 167-Hz stimuli. For each antenna or $TiCl_4$ recording, the onset was defined as the time point where the mean and SD of the signal to the first pulse in each of 10 stimuli was greater than (and stayed above for at least 1 ms to avoid false onsets) 2.5 times the SD of the signal during the first 3 ms after valve trigger (12 points).

Periodograms were estimated by using Welch's method with 90% overlap and 1-s window size. Odor-evoked periodograms were calculated for single recordings by subtracting the periodogram derived from the EAG response to the blank control from the periodogram derived from the EAG response to the odor stimulus.

The periodogram in Fig. S1*D* was constructed from the final 9 s of 10-s stimuli to capture steady-state dynamics.

Coherence between the averaged, blank corrected responses to odor stimulus and to the averaged $TiCl_4$ smoke signal (recorded on separate trials in response to the same stimulus) was computed by using 265-ms segments (1,000 samples after 8× down-sampling) with 50% overlap. Blank subtraction occurred in the time domain. Confidence intervals were computed by creating shuffles of the $TiCl_4$ signal. The shuffle procedure consisted of randomizing phases in the frequency domain but maintaining an identical power spectrum. The SD of the coherence spectrum across shuffles was used as an estimate of the SD of the unshuffled coherence. Coherograms were computed by using a sliding coherence estimate, with 1-s windows and 95% overlap. Within each window, the coherence was estimated by using 50-ms subwindows and 95% overlap.

ACKNOWLEDGMENTS. We thank Elizabeth Cash, Meghan E. Duell, Cécile P. Faucher, Hong Lei, Danielle Protas, and Zachary Shaffer for insects supply; Cécile P. Faucher and Hong Lei for Manduca sex pheromone; Cornelis Klok and Benjamin Paffhausen for technical support; and John G. Hildebrand, Ramón Huerta, Christopher Jernigan, Christoph J. Kleineidam, and Irina Sinakevitch for discussions. This work was financially supported by the Bundesministerium für Bildung und Forschung Grant 01GQ0931 (to P.S. and C.G.G.) and by Deutsche Forschungsgemeinschaft Priority Program SPP1392 (to C.G.G.).

1. Murlis J, Elkinton JS, Carde RT (1992) Odor plumes and how insects use them. *Annu Rev Entomol* 37:505–532.
2. Baker TC, Fadamiro HY, Cosse AA (1998) Moth uses fine tuning for odour resolution. *Nature* 393(6685):530.
3. Fadamiro HY, Cosse AA, Baker TC (1999) Fine-scale resolution of closely spaced pheromone and antagonist filaments by flying male Helicoverpa zea. *J Comp Physiol A Neuroethol Sens Neural Behav Physiol* 185(2):131–141.
4. Nikonov AA, Leal WS (2002) Peripheral coding of sex pheromone and a behavioral antagonist in the Japanese beetle, Popillia japonica. *J Chem Ecol* 28(5):1075–1089.
5. Andersson MN, Binyameen M, Sadek MM, Schlyter F (2011) Attraction modulated by spacing of pheromone components and anti-attractants in a bark beetle and a moth. *J Chem Ecol* 37(8):899–911.
6. Szyszka P, Stierle JS, Biergans S, Galizia CG (2012) The speed of smell: Odor-object segregation within milliseconds. *PLoS ONE* 7(4):e36096.
7. Stierle JS, Galizia CG, Szyszka P (2013) Millisecond stimulus onset-asynchrony enhances information about components in an odor mixture. *J Neurosci* 33(14):6060–6069.
8. Schneider D, Lacher V, Kaissling KE (1964) Die Reaktionsweise und das Reaktionsspektrum von Riechzellen bei Antheraea pernyi (Lepidoptera, Saturniidae). *Z Vgl Physiol* 48(6):632–662.
9. de Bruyne M, Clyne PJ, Carlson JR (1999) Odor coding in a model olfactory organ: The Drosophila maxillary palp. *J Neurosci* 19(11):4520–4532.
10. Sato K, et al. (2008) Insect olfactory receptors are heteromeric ligand-gated ion channels. *Nature* 452(7190):1002–1006.
11. Kaissling KE (2013) Kinetics of olfactory responses might largely depend on the odorant-receptor interaction and the odorant deactivation postulated for flux detectors. *J Comp Physiol A Neuroethol Sens Neural Behav Physiol* 199(11):879–896.
12. Lemon W, Getz W (1997) Temporal resolution of general odor pulses by olfactory sensory neurons in American cockroaches. *J Exp Biol* 200(Pt 12):1809–1819.
13. Bau J, Justus KA, Cardé RT (2002) Antennal resolution of pulsed pheromone plumes in three moth species. *J Insect Physiol* 48(4):433–442.
14. Hinterwirth A, Zeiner R, Tichy H (2004) Olfactory receptor cells on the cockroach antennae: Responses to the direction and rate of change in food odour concentration. *Eur J Neurosci* 19(12):3389–3392.
15. Justus KA, Cardé RT, French AS (2005) Dynamic properties of antennal responses to pheromone in two moth species. *J Neurophysiol* 93(4):2233–2239.
16. Schuckel J, Meisner S, Torkkeli PH, French AS (2008) Dynamic properties of Drosophila olfactory electroantennograms. *J Comp Physiol A Neuroethol Sens Neural Behav Physiol* 194(5):483–489.
17. Tripathy SJ, et al. (2010) Odors pulsed at wing beat frequencies are tracked by primary olfactory networks and enhance odor detection. *Front Cell Neurosci* 4:1.
18. Kim AJ, Lazar AA, Slutskiy YB (2011) System identification of Drosophila olfactory sensory neurons. *J Comput Neurosci* 30(1):143–161.
19. French AS, Meisner S, Su CY, Torkkeli PH (2014) Carbon dioxide and fruit odor transduction in Drosophila olfactory neurons. What controls their dynamic properties? *PLoS ONE* 9(1):e86347.
20. Mayer MS, Mankin RW, Lemire GF (1984) Quantitation of the insect electroantennogram - measurement of sensillar contributions, elimination of background potentials, and relationship to olfactory sensation. *J Insect Physiol* 30(9):757–763.
21. Kapitskii SV, Gribakin FG (1992) Electroantennogram of the American cockroach: Effect of oxygen and an electrical model. *J Comp Physiol A Neuroethol Sens Neural Behav Physiol* 170(5):651–663.
22. Nagel KI, Wilson RI (2011) Biophysical mechanisms underlying olfactory receptor neuron dynamics. *Nat Neurosci* 14(2):208–216.
23. Martelli C, Carlson JR, Emonet T (2013) Intensity invariant dynamics and odor-specific latencies in olfactory receptor neuron response. *J Neurosci* 33(15):6285–6297.
24. Silbering AF, Benton R (2010) Ionotropic and metabotropic mechanisms in chemoreception: 'Chance or design'? *EMBO Rep* 11(3):173–179.
25. Leal WS (2013) Odorant reception in insects: Roles of receptors, binding proteins, and degrading enzymes. *Annu Rev Entomol* 58:373–391.
26. Kanaujia S, Kaissling KE (1985) Interactions of pheromone with moth antennae - adsorption, desorption and transport. *J Insect Physiol* 31(1):71–81.
27. Steinbrecht RA (1997) Pore structures in insect olfactory sensilla: A review of data and concepts. *Int J Insect Morphol* 26(3-4):229–245.
28. Maitani MM, Allara DL, Park KC, Lee SG, Baker TC (2010) Moth olfactory trichoid sensilla exhibit nanoscale-level heterogeneity in surface lipid properties. *Arthropod Struct Dev* 39(1):1–16.
29. Vogt RG, Riddiford LM (1981) Pheromone binding and inactivation by moth antennae. *Nature* 293(5828):161–163.
30. Vogt RG, Callahan FE, Rogers ME, Dickens JC (1999) Odorant binding protein diversity and distribution among the insect orders, as indicated by LAP, an OBP-related protein of the true bug Lygus lineolaris (Hemiptera, Heteroptera). *Chem Senses* 24(5):481–495.
31. Wicher D, et al. (2008) Drosophila odorant receptors are both ligand-gated and cyclic-nucleotide-activated cation channels. *Nature* 452(7190):1007–1011.
32. Ignatious Raja JS, Katanayeva N, Katanaev VL, Galizia CG (2014) Role of $G_{o/i}$ subgroup of G proteins in olfactory signaling of Drosophila melanogaster. *Eur J Neurosci* 39(8):1245–1255.
33. Niven JE, Anderson JC, Laughlin SB (2007) Fly photoreceptors demonstrate energy-information trade-offs in neural coding. *PLoS Biol* 5(4):e116.
34. Firestein S, Shepherd GM, Werblin FS (1990) Time course of the membrane current underlying sensory transduction in salamander olfactory receptor neurones. *J Physiol* 430:135–158.
35. Sato K, Suzuki N (2000) The contribution of a $Ca^{(2+)}$-activated $Cl^{(-)}$ conductance to amino-acid-induced inward current responses of ciliated olfactory neurons of the rainbow trout. *J Exp Biol* 203(Pt 2):253–262.
36. Hardie RC, Raghu P (2001) Visual transduction in Drosophila. *Nature* 413(6852):186–193.
37. Wever E, Bray C (1937) The perception of low tones and the resonance-volley theory. *J Psychol* 3(1):101–114.
38. Schuckel J, Torkkeli PH, French AS (2009) Two interacting olfactory transduction mechanisms have linked polarities and dynamics in Drosophila melanogaster antennal basiconic sensilla neurons. *J Neurophysiol* 102(1):214–223.
39. Getahun MN, Wicher D, Hansson BS, Olsson SB (2012) Temporal response dynamics of Drosophila olfactory sensory neurons depends on receptor type and response polarity. *Front Cell Neurosci* 6:54.
40. Christensen TA, Hildebrand JG (1988) Frequency coding by central olfactory neurons in the sphinx moth Manduca sexta. *Chem Senses* 13(1):123–130.
41. Heinbockel T, Christensen TA, Hildebrand JG (1999) Temporal tuning of odor responses in pheromone-responsive projection neurons in the brain of the sphinx moth Manduca sexta. *J Comp Neurol* 409(1):1–12.
42. Vickers NJ (2000) Mechanisms of animal navigation in odor plumes. *Biol Bull* 198(2):203–212.
43. Riffell JA, et al. (2014) Sensory biology. Flower discrimination by pollinators in a dynamic chemical environment. *Science* 344(6191):1515–1518.
44. Hopfield JF, Gelperin A (1989) Differential conditioning to a compound stimulus and its components in the terrestrial mollusc Limax maximus. *Behav Neurosci* 103(2):5.
45. Broome BM, Jayaraman V, Laurent G (2006) Encoding and decoding of overlapping odor sequences. *Neuron* 51(4):467–482.
46. Saha D, et al. (2013) A spatiotemporal coding mechanism for background-invariant odor recognition. *Nat Neurosci* 16(12):1830–1839.
47. Wachowiak M (2011) All in a sniff: Olfaction as a model for active sensing. *Neuron* 71(6):962–973.
48. Mozell MM (1970) Evidence for a chromatographic model of olfaction. *J Gen Physiol* 56(1):46–63.
49. Nowotny T, Stierle JS, Galizia CG, Szyszka P (2013) Data-driven honeybee antennal lobe model suggests how stimulus-onset asynchrony can aid odour segregation. *Brain Res* 1536:119–134.
50. Muezzinoglu MK, et al. (2009) Acceleration of chemo-sensory information processing using transient features. *Sens Actuators B Chem* 137(2):507–512.
51. Myrick AJ, Baker TC (2011) Locating a compact odor source using a four-channel insect electroantennogram sensor. *Bioinspir Biomim* 6(1):016002.
52. Kanzaki R, Minegishi R, Namiki S, Ando N (2013) Insect-machine hybrid system for understanding and evaluating sensory-motor control by sex pheromone in Bombyx mori. *J Comp Physiol A Neuroethol Sens Neural Behav Physiol* 199(11):1037–1052.
53. Martinez D, Arhidi L, Demondion E, Masson JB, Lucas P (2014) Using insect electroantennogram sensors on autonomous robots for olfactory searches. *J Vis Exp* (90):e51704.